JACS
JOURNAL OF THE AMERICAN CHEMICAL SOCIETY
pubs.acs.org/JACS
Article

Plateau–Rayleigh Instability in Soft-Lattice Inorganic Solids

Zhen-Chao Shao,[§] Xianyun Jiang,[§] Chong Zhang,[§] Tianhao Wang, Yan-Ru Wang, Guo-Qiang Liu, Zong-Ying Huang, Yu-Zhuo Zhang, Liang Wu, Zhong-Huai Hou, Huijun Jiang,* Yi Li,* and Shu-Hong Yu*

Cite This: https://doi.org/10.1021/jacs.4c11866

ABSTRACT: Plateau–Rayleigh instability—a macroscopic phenomenon describing the volume-constant breakup of one-dimensional continuous fluids—has now been widely observed in adatoms, liquids, polymers, and liquid metals. This instability enables controlled wetting–dewetting behavior at fluid–solid interfaces and, thereby, the self-limited patterning into ordered structures. However, it has yet to be observed in conventional inorganic solids, as the rigid lattices restrict their "fluidity". Here, we report the general fluid-like Plateau–Rayleigh instability of silver-based chalcogenide semiconductors featuring soft-lattice ionic crystals. It enables postsynthetic morphing from conformal core–shell nanowires to periodically coaxial ones. We reveal that such self-limited reconstruction is thermodynamically driven by the surface energy and interface energy and kinetically favored by the high ionic diffusion coefficients of subnanoscale soft-lattice shells. The resulting periodic heterostructures can be topotactically transformed for epitaxial combinations of functional semiconductors free from the lattice-matching rule. This fluid-like behavior in soft inorganic solids thus offers routes toward sophisticated nanostructures and controllable patterning at all-inorganic solid–solid interfaces.

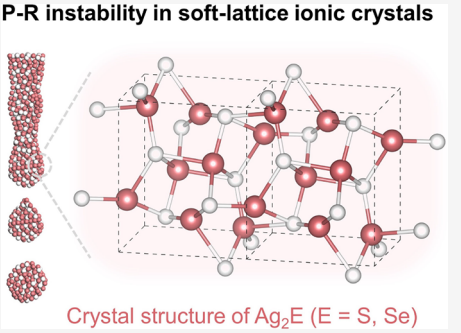

INTRODUCTION

The wetting–dewetting behavior at the two-phase interface—a universal property in nature—is widely observed for liquids in desert beetles,[1] spider silk,[2] and lotus leaves,[3] among others. These fascinating phenomena have now boomed a new field of biomimic interfacial engineering, in which the ability to control their wetting–dewetting process in a predictable and generalizable manner would have significant implications for many applications.[4,5]

Specifically, the wetting–dewetting behavior for matters on one-dimensional (1D) substrates is known as the Plateau–Rayleigh (P-R) instability (Figure 1a and Video S1)—a macroscopic phenomenon found in the 1800s that describes the volume-constant breakup of a continuous water cylinder into isolated droplets as driven by the surface tension.[6,7] More generally, P-R instability has now been extended to a broad range of artificial 1D viscous fluids—even at the nanoscale—including adatoms,[8,9] liquids,[10−12] polymers,[13−15] and liquid metals.[16−18] These instabilities that enable transformations into uniform droplets, ordered microparticles, and periodic fibrous structures now find practical applications in liquid dispensers,[19] inject printers,[20,21] microfluidics,[22] water collectors,[23,24] sensors,[25] and photonics.[8,26]

However, P-R instability has not been found in conventional inorganic solids (Figure 1b). Unlike the soft viscous fluids, it requires repetitive debonding and bonding in these rigid, brittle lattices to ensure their "fluidity" on substrates, which seems impossible for conventional inorganic solids unless melted. In fact, controlling the wetting–dewetting behavior of inorganic solids would be more than important for directly engineering the patterning and ordering of all-inorganic components.[27,28] In particular, by carefully managing their interfacial wettability at the nanoscale, we are then capable of patterning different functional subunits into high-order nanostructures with well-defined compositions, structures, interfaces, and spatial arrangements, for instance, periodic heteronanowires. Benefiting from improved optical absorption, mitigated interfacial defects, engineerable band structures, and steerable carrier transport,[29,30] they hold exciting promises for applications in catalysis,[31] optoelectronics,[32] and solar conversion.[29,30,33] In this respect, the inaccessibility of P-R instability in inorganic solids has largely impeded the path toward ordered patterns at artificial inorganic interfaces[27,28] and toward high-order periodic nanostructures with improved or new functions.[30,32,34]

Here, we present a new twist on this issue by demonstrating the first observation of solid-state P-R instability in a class of soft-lattice metastable ionic crystals. The inherently weak atomic interactions and highly mobile cations therein allow fast

Received: August 29, 2024
Revised: November 8, 2024
Accepted: November 12, 2024

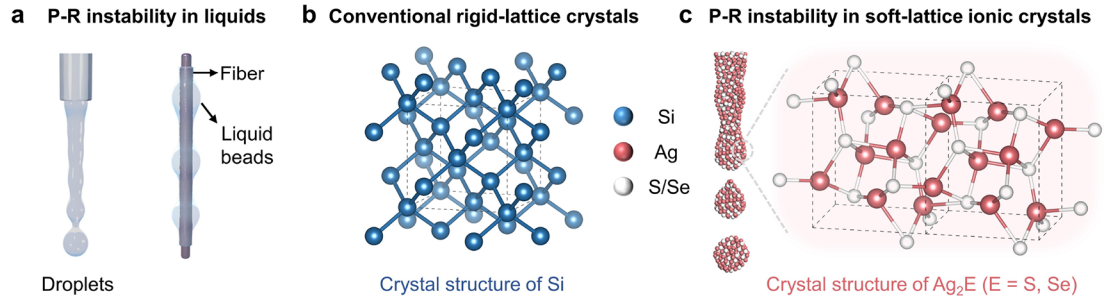

Figure 1. Schematics of liquid- and solid-state P-R instability. (a) Two types of P-R instability in liquids: falling droplets and beads on the fiber. (b) Representative rigid-lattice crystal of Si. (c) P-R instability in Ag_2E (E = S, or Se) soft-lattice ionic crystals.

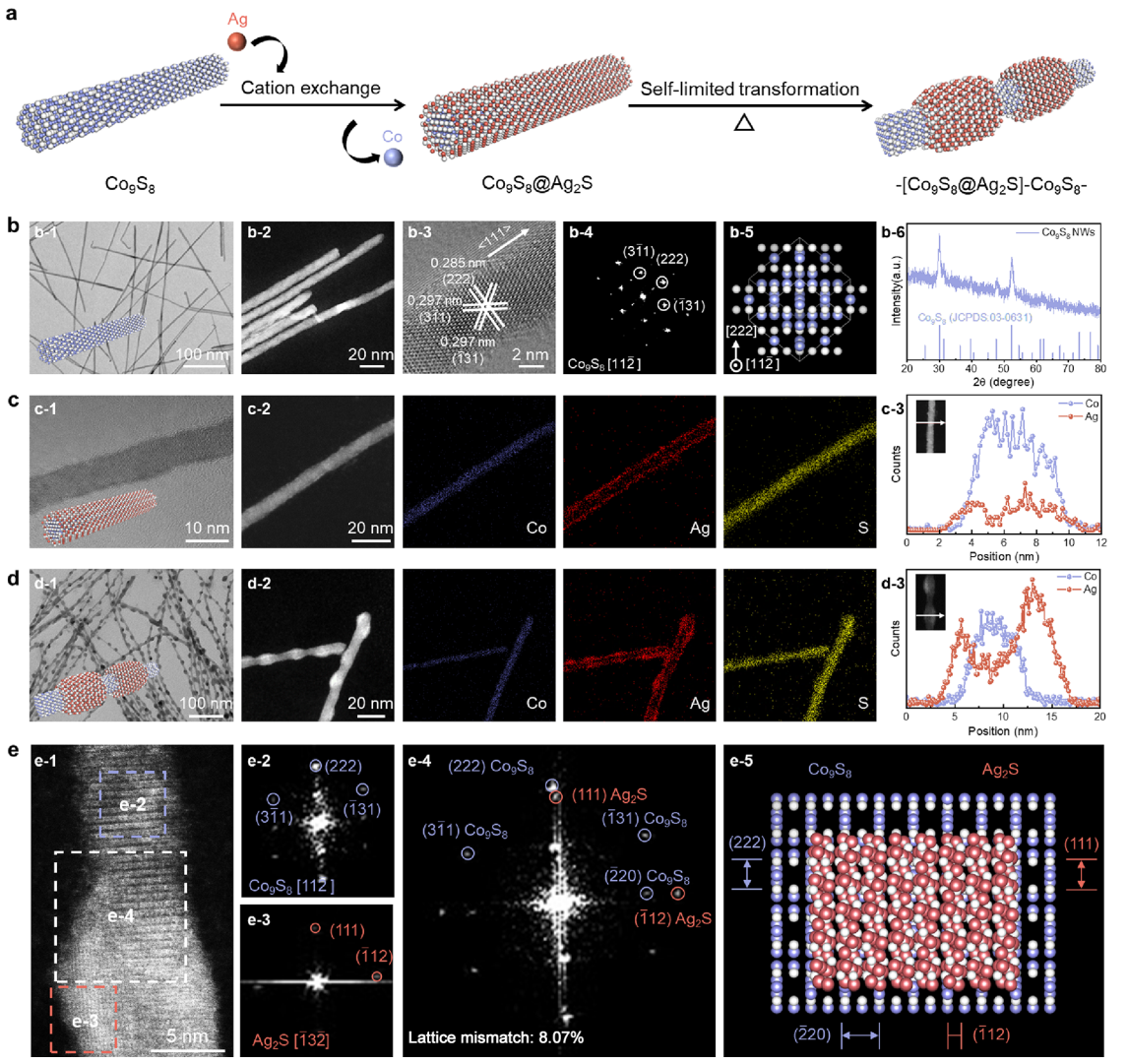

Figure 2. Plateau−Rayleigh (P-R) instability in soft-lattice Ag_2S shells enables periodically coaxial heteronanowires. (a) P-R instability in solids, by which cation-exchanged Co_9S_8@Ag_2S conformal core−shell heteronanowires self-limitedly transform into −[Co_9S_8@Ag_2S]-Co_9S_8− periodically coaxial ones. (b) Characterization of Co_9S_8 nanowires. (b-1) TEM image. (b-2) HAADF-STEM image. (b-3) HRTEM image. (b-4) Corresponding FFT image. (b-5) Atomic model with the same orientation as the FFT image. (b-6) XRD pattern corresponding to cubic-phase Co_9S_8. (c, d) Characterization of Co_9S_8@Ag_2S heteronanowires and −[Co_9S_8@Ag_2S]-Co_9S_8− heteronanowires. (c-1, d-1) TEM image. (c-2, d-2) HAADF-STEM and EDS elemental mapping images. (c-3, d-3) EDS line-scan profiles. (e) Characterization of the Co_9S_8/Ag_2S heterointerface. (e-1) High-resolution HAADF-STEM image of −[Co_9S_8@Ag_2S]-Co_9S_8− heteronanowires. (e-2, e-3, e-4) FFT images corresponding to three dashed squares in (e-1), showing the epitaxial relationship between Co_9S_8 core and Ag_2S shell. (e-5) Atomic model of the Co_9S_8/Ag_2S heterointerface with the same orientation as the FFT image in (e-4).

breaking and reformation of these ionic bonds (Table S1).[35−38] As a consequence, they can dynamically behave as "soft viscous solids" and hold promise to realize the fluid-like P-R instability in a thermodynamic landscape (Figure 1c).

https://doi.org/10.1021/jacs.4c11866
J. Am. Chem. Soc. XXXX, XXX, XXX−XXX

We showcase the P-R instability in silver-based chalcogenide semiconductors Ag_2E (E = S or Se) featuring soft ionic lattices, which make up an important class of transformative reaction intermediates for colloidal nanocrystals. Due to the instability, preformed Ag_2E shells with uniform subnanometer-thickness wetting on core nanowires (e.g., Co_9S_8, ZnS, and ZnSe)—a configuration we term conformal core−shell heteronanowires—can postsynthetically dewet into periodic shells (i.e., periodically coaxial heteronanowires) in a controlled manner. Different from prior surface-energy-modulated P-R instability in single-component fluids, the self-limited transformation of such heteronanowires here is revealed to be an outcome of the minimization of the surface energy and interface energy. Meanwhile, the high ionic diffusion coefficients in such soft-lattice ultrathin shells ensure that the transformation is kinetically accessible. As key reaction intermediates, these resulting high-order periodic nanostructures then further enable topotactic transformations. We epitaxially integrate therein a library of functional semiconductor subunits free from the lattice-matching requirement and, consequently as demonstrated, achieve improved solar energy conversion.

RESULTS AND DISCUSSION

Morphological Transformation Based on Solid-State P-R Instability. To realize the P-R instability, we first sought 1D nanowire substrates capable of forming the conformal core−shell structure when introducing soft Ag^+ ions therein. Considering the relatively large ionic radii of Ag^+ (Table S2),[39] we postulated that semiconductor nanowires with cations of small ionic radii, such as cobalt sulfides, may enable expelling incompatible Ag^+ in the solid lattices outsides, therefore forming core−shell structures instead of the doped or alloyed ones.[23] We thus developed a facile catalyzed growth strategy for the one-pot synthesis of high-quality Co_9S_8 nanowires, which can serve as 1D substrates for the further observation of solid-state P-R instability (Figure 2a).

Figure S1a illustrates the solution-solid−solid growth mechanism of Co_9S_8 nanowires using superionic Ag_2S tips as the solid catalysts (see the Experimental Section for synthetic details). The high stability of such solid catalysts can, in principle, allow diameter- and length-controlled growth of monodispersed nanowires.[40] Transmission electron microscopy (TEM) images (Figure 2b-1 and Figure S1b) and high-angle annular dark-field scanning TEM (HAADF-STEM) images (Figure 2b-2 and Figure S1c,d) confirmed the high uniformity of the resulting Ag_2S-tipped Co_9S_8 nanowires. The length of such high-quality nanowires can be modulated from sub-100 nm to micrometers by controlling the reaction time (Figure S1e,f), and the diameter of nanowires is estimated to be 8.18 ± 1.57 nm depending on the reaction temperature (Figure S1g). The typical high-resolution TEM (HRTEM) images (Figure 2b-3 and Figure S1h) and corresponding fast Fourier transform (FFT) images (Figure 2b-4 and Figure S1i) revealed the cubic-phase structure of Co_9S_8 nanowires that grow along the ⟨111⟩ crystallographic orientation, a result that coincides well with the oriented atomic model (Figure 2b-5) and power X-ray diffraction (PXRD) pattern (Figure 2b-6). The energy dispersive X-ray spectroscopy (EDS) elemental mapping images (Figures S1j and S2) further confirmed the uniform distribution of Co and S throughout the nanowire, with Ag_2S at the apex. X-ray photoelectron spectroscopy (XPS) verified the coexistence of both Co^{2+} and Co^{3+} with a slight amount of Ag^+ due to the presence of small Ag_2S tips (Figure S3).

To demonstrate the P-R instability of metastable silver-based chalcogenides, we then constructed the Co_9S_8@Ag_2S conformal core−shell heteronanowires via room-temperature cation exchange reactions, which were further postsynthetically transformed into the −[Co_9S_8@Ag_2S]-Co_9S_8− periodically coaxial heteronanowires upon heating.

According to the Pearson's hard−soft acid−base (HSAB) theory,[35] the cation exchange reaction between Co_9S_8 nanowires and soft-acid Ag^+ is feasible because both Co^{2+} and Co^{3+} are harder than Ag^+. Instead of a morphology-conserved homogeneous reaction within the nanowires as observed for conventional colloidal nanocrystals, the nanowires presented here were converted into heterostructures with a uniform shell of subnanometer thickness, as shown in Figure 2c-1 and Figure S4a,b. The formation of such conformal core−shell structures holds true even with an excess of Ag^+ introduced in the reaction solution (Figure S5), suggesting that the reaction is a self-limited process—a finding we attribute to the low Ag^+ dopant tolerance in Co_9S_8 lattices due to the large ionic radius difference of the two cations.

We further confirmed the conformal core−shell structures of Co_9S_8@Ag_2S nanowires via the HAADF-STEM images, EDS elemental mapping images, and line-scan profiles (Figure 2c-2,c-3 and Figure S4c−e), wherein an ultrathin shell of Ag_2S uniformly distribute on the Co_9S_8 nanowires. The average thickness of the Ag_2S shells was statistically estimated to be 1.02 ± 0.20 nm (Figure S 4f). The high-resolution HAADF-STEM images and corresponding FFT images (Figure S6) indicate that the crystal structure and growth orientation of Co_9S_8 nanowires remain unchanged after the cation exchange reaction, whereas the lattice of subnanometer-thickness Ag_2S shells is severely distorted because of the large interfacial strain.

Low lattice energies and high-mobility cations of metastable Ag_2S ionic crystals make the Ag_2S shells highly deformable,[35−37,41] which are thus capable of presenting the liquid-like P-R instability and slowly dewetting into periodic shells at room temperature (Figure S7). By accelerating the dewetting process, the core−shell Co_9S_8@Ag_2S heteronanowires dispersed in toluene postsynthetically transformed into the −[Co_9S_8@Ag_2S]-Co_9S_8− periodically coaxial heteronanowires after keeping it at 60 °C for 12 h. As shown in the TEM images (Figure 2d-1 and Figure S8a) and HAADF-STEM images (Figure 2d-2 and Figure S8b), Ag_2S shells with higher contrast segmentally distribute along Co_9S_8 nanowires in the form of a necklace-like configuration. The EDS mapping images (Figure 2d-2 and Figure S8d) and line-scan profiles (Figure 2d-3 and Figure S8e,f) further demonstrate that the Ag_2S shell coating outside of Co_9S_8 tends to segregate from an ultrathin, uniform one to a thick, periodic one, finally yielding the periodically coaxial structures with well-defined heterointerfaces. The thickness of the periodic shell is estimated to be around 4.94 ± 1.03 nm (Figure S8c). Despite such thickness variation, the mass of Ag_2S shells were quantified to keep constant before and after the transformation (Table S3), in line with the volume-constant P-R process.

According to the PXRD pattern (Figure S8g), the Ag_2S shells stabilize with a monoclinic phase (JCPDS card: 89-3840) in the resulting periodic structures. The atom-resolution HAADF-STEM image of the [Co_9S_8@Ag_2S]-Co_9S_8 segments then further reveals the crystallographic orientation at the Ag_2S-Co_9S_8 heterointerfaces (Figure 2e-1). FFT images corresponding to the Co_9S_8 subunit (Figure 2e-2), Ag_2S subunit (Figure 2e-3), and Co_9S_8/Ag_2S heterointerface (Figure 2e-4) suggest the epitaxial relationship for the (222)Co_9S_8/(111)Ag_2S hetero-

https://doi.org/10.1021/jacs.4c11866
J. Am. Chem. Soc. XXXX, XXX, XXX−XXX

interface (Figure 2e-5). The lattice mismatch of 8.07% therein may contribute to the formation of such periodic coaxial structure, which allows to reduce the interface strain as compared with the conformal one.

In-Situ/Ex-Situ Observations and Underlying Mechanisms. To have a closer look at such P-R instability of nanoscale inorganic solids, we tracked the time-dependent morphological evolution via both in-situ and ex-situ TEM images. In-situ TEM images were collected by heating the conformal core−shell nanowires on holey carbon-coated SiC substrates at 180 °C (Figure 3a). We note that the periodically coaxial nanowires can

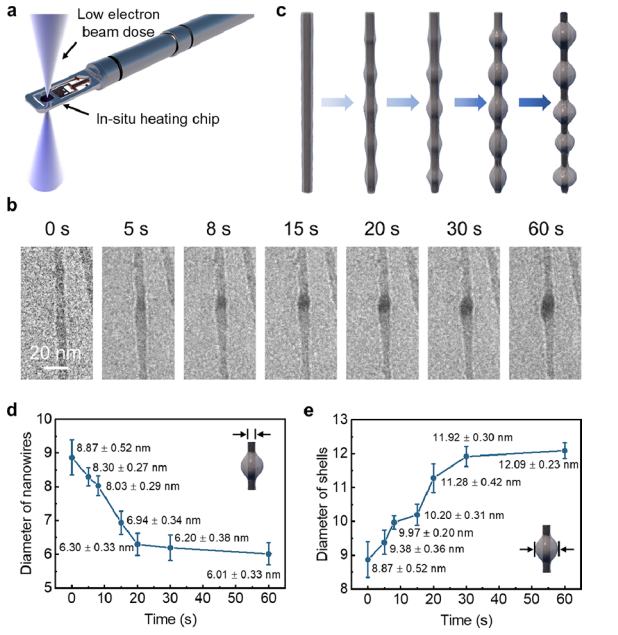

Figure 3. In situ heating experiment of the solid-state P-R instability. (a) Schematic illustration of the in situ heating experiment. (b) In situ TEM images of heteronanowires at different heating times. (c) Schematic illustration of the self-limited transformation process due to solid-state P-R instability. (d, e) Time-dependent evolutions of the nanowire diameters (d) and shell diameters (e).

be achieved as well by heating the solid-state conformal core−shell nanowires on substrates (Figure S9). This indicates that the transformation of Ag_2S shells is a self-limited on-nanowire process irrelevant to the solvents, which ensures the accessibility of in situ solid observation.

Generally, the heterogeneous growth modes of two chemically and structurally distinct materials can be described by the total Gibbs free energy change of the system, ΔE_{total}, that is, a sum of surface and interface energy differences (Figure S10).[42,43] By *in-situ* heating conformal core−shell nanowires for different times (Figure 3b, Figures S11 and S12, and Videos S2 and S3), we found that the uniform Ag_2S shells (Frank−Van der Merwe mode for $\Delta E_{total} > 0$) gradually dewet into islands-on-slabs (Stranski−Krastanov mode for the intermediate state) and finally stabilize as isolated shells of larger sizes (Volmer−Weber mode for $\Delta E_{total} < 0$), as schematically illustrated in Figure 3c. The P-R instability is characterized by the time-dependent decrease of nanowire diameters in the conformal segments (Figure 3d) and the increase of diameters in the $-[Co_9S_8@Ag_2S]-$ shell segments (Figure 3e), wherein the ultrathin Ag_2S shell diffuses and segregates into larger ones. Therefore, the evolution of growth modes suggests it as an energetically preferred spontaneous process from metastable to thermodynamically stable processes (Figure S13). The mild heating in experiment mainly assists in overcoming the relatively low kinetic energy barrier for transformation. As a result, we are even capable of realizing the direct synthesis of periodic nanowires by conducting the cation exchange reaction at a modest temperature of 80 °C for 10 min (Figure S14).

We then further quantified the self-limited transformation process via ex-situ TEM observation. We synthesized a series of conformal core−shell nanowires with tunable shell thicknesses by changing the amount of $AgNO_3$ in the cation exchange reaction (Figure 4a and Figure S15). The time-dependent size

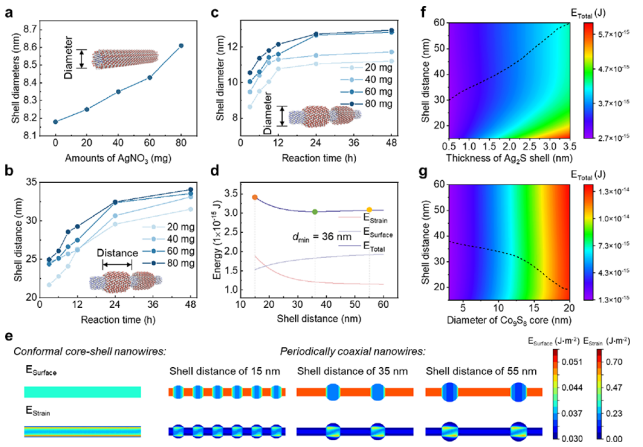

Figure 4. Thermodynamic analyses on the solid-state P-R instability. (a) Statistical diameter evolution of core−shell $Co_9S_8@Ag_2S$ heteronanowires with different thicknesses of Ag_2S shells. (b, c) Time-dependent evolutions of distances (b) and diameters (c) for Ag_2S shells starting from different conformal nanowires in (a). (d) Calculated strain energy, surface energy, and total Gibbs free energy for the periodically coaxial heteronanowires with different shell distances. (e) Projected surface and strain energy distributions in different theoretical models. (f, g) Calculated landscapes of total Gibbs free energies for $-[Co_9S_8@Ag_2S]-Co_9S_8-$ periodically coaxial heteronanowires with varied thicknesses of Ag_2S shells (f) and Co_9S_8 cores (g). The dashed lines refer to the corresponding d_{min} values for different nanowires.

evolutions of these nanowires upon heating were then tracked and quantified using ex-situ TEM images (Figures S16−S19). The tendencies are of high consistency with the P-R instability (Figure 4b,c): (1) by keeping the shell volume constant, all conformal core−shell nanowires gradually transform into periodically coaxial ones with increased shell distances and diameters as the heating proceeds, which eventually stabilize at equilibrium states; (2) increasing the thickness of initial Ag_2S shells produces periodic shells with larger distances and diameters.

In fact, the observation of P-R instability in inorganic solids is amazing yet exciting. Inorganic solids, such as semiconductors and ceramic insulators, are usually known to be rigid and brittle as a result of their strong ionic or directional covalent bonds, which do not deform easily. Despite that a very few of soft-lattice crystals have shown intrinsic plasticity and deformability in bulk,[37,44−46] the fluidity of inorganic crystals has yet to be revealed. To understand the underlying driving forces enabling such self-limited transformation, we then studied, with respect to thermodynamics, the surface and interface energies in these structures before and after the transformation.

https://doi.org/10.1021/jacs.4c11866
J. Am. Chem. Soc. XXXX, XXX, XXX−XXX

We thus provide a thermodynamic landscape of the Co_9S_8@Ag_2S core−shell structures via finite element analysis (Note S1). We assume that the total volume of the Ag_2S shells remains constant during the morphological transformation. As such, by changing the size parameters of the core−shell structures, we calculated both the interface and surface energies of each configuration, which constitute the total Gibbs free energy of the system, E_{Total}.

The interface energy, as manifested by the interface strain of inorganic solids, positively correlates with the lattice mismatch between two heterogeneous components. Starting from initially conformal nanowires with the core diameter of 6.4 nm and shell thickness of 1.0 nm, we show that as the distance of two adjacent Ag_2S shells increases, the interface strain energy decreases accordingly (Figure 4d and Figure S20), a finding consistent with the crystallographic analysis as discussed in Figure 2e. Note that the distance of 0 nm corresponds to the conformal structure with a uniform Ag_2S shell along the nanowire, which exhibits the highest E_{Total} dominated by the interface strain energy (Figure S20). In parallel, the surface energy is found to monotonically increase with shell distance. Therefore, as a sum of the surface and interface strain energies, E_{Total} exhibits a minimum at a shell distance of around 36 nm (denoted as d_{min}), a value close to the experimental ones. The configuration at d_{min} thus represents the thermodynamically stable state for periodically coaxial nanowires.

To reveal the origins of these energetic evolutions, we provide the cross profiles of elastic strain tensors (Figure S21a) as well as the projected distributions of strain and surface energy in theoretical models of different shell distances (Figure 4e and Figure S21b,c). As shown, the lattice mismatch leads to compressive stress on the Ag_2S shell and tensile stress on the Co_9S_8 core, which all concentrate at the heterointerfaces. In this way, the total strain energy of heteronanowires dictated by the interface area decreases with a larger shell distance, despite the fact that the strain energy at each heterointerface is larger, whereas the surface energy is mainly contributed by the high-energy Co_9S_8 cores and, thereby, increases with a larger shell distance by exposing more Co_9S_8 outsides. As a result, the opposite dependences on shell distances for strain energy and surface energy lead to a thermodynamically stable configuration at d_{min}. The calculation results interpret well the self-limited transformation as a combinatorial, spontaneous outcome of surface and interface energy changes, according well with the TEM observations for cases from $\Delta E_{Total} > 0$ to $\Delta E_{Total} < 0$.

We further show that the island-like shell distance is highly tunable by changing the core diameters and shell thicknesses of initial conformal structures. First, when keeping the diameter of Co_9S_8 cores constant, the energy landscape indicates that d_{min} increases with the initial shell thickness and gradually reaches an equilibrium (Figure 4f and Figure S22a,b)—a tendency matches well with the experimental ones (Figure 4b,c). This occurs because the P-R instability is dominated by the strain energy of shells, which prefer to repel each other into a large shell distance to reduce the strain energy. Second, when keeping the thickness of Ag_2S shells constant, d_{min} decreases with the core diameter (Figure 4g and Figure S22c,d). Accordingly, we experimentally validated this tendency by using Co_9S_8 nanowires of a larger diameter for reactions, which finally produced periodic heteronanowires of smaller shell distances (Figure S23). Third, to examine the influence of the ratio of shell thickness to core diameter, we further calculated the energy evolution and thermodynamically stable structures for different conformal core−shell nanowires with the same shell-to-core size ratio (Figure S24). Consequently, d_{min} varied from 35 to 38 nm when their initial sizes increased by 0.75, 1, 1.25, and 1.5 times. This implies that, instead of the shell-to-core size ratios, the P-R instability is in fact controlled by their absolute sizes of initial core−shell nanowires, because the strain energy scales with the volume of the model and the surface energy is related to its surface area.

Despite the thermodynamic accessibility for the P-R instability in solids, the kinetic understanding of the "liquid-like fluidity" in such kind of soft-lattice ionic crystals that are unattainable for conventional rigid solids remains unclear. To this end, molecular dynamics simulations were employed to quantify the "fluidity" of Ag_2S shells of different thicknesses (0.5−10.0 nm) on a stable, oriented Co_9S_8 substrate (Note S2). Thanks to the weak atomic interactions in the soft-lattice ionic crystals, we found that Ag^+ and S^{2-} therein are highly mobile, as reflected by the mean square displacements (MSDs) and corresponding diffusion coefficients (D) (Figure 5a−d).

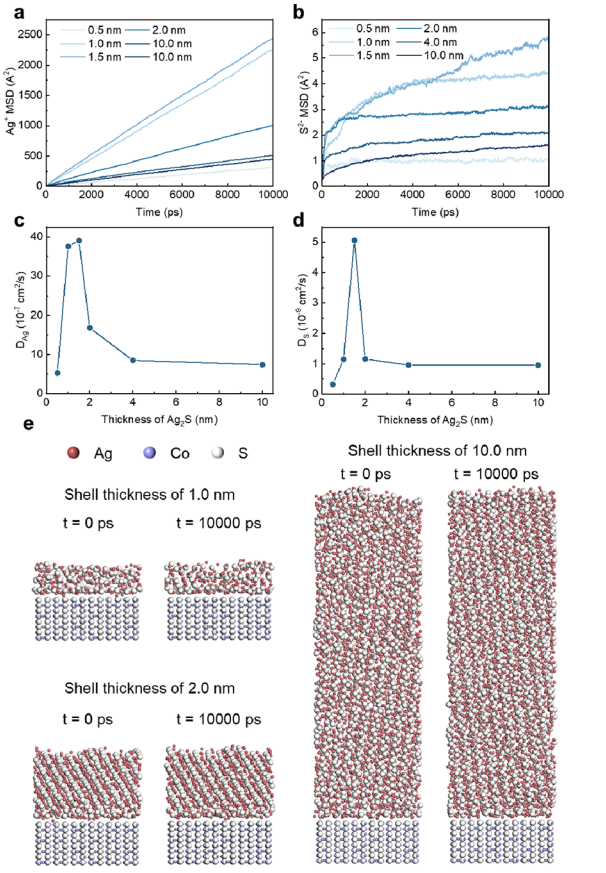

Figure 5. Molecular dynamics simulations. (a, b) Mean square displacements (MSD) of Ag^+ (a) and S^{2-} (b) in molecular dynamics simulations. (c, d) Diffusion coefficients (D) of Ag^+ (c) and S^{2-} (d). (e) Snapshots of Ag_2S shells with different thicknesses (1.0 2.0, and 10.0 nm) at different times (t = 0 and 10,000 ps).

Both D_S and D_{Ag} exhibit volcano-shaped relationships as the thickness of Ag_2S shell increases and reach their maximal values for those with subnanometer thicknesses. The Ag_2S lattices stay almost fixed with bulk-like features when the thicknesses are below 0.5 nm and approach 10.0 nm, because atoms adjacent to the substrate and far from the substrate are restrained by the Co_9S_8 lattice and the Ag_2S bulk lattice, respectively (Figure 5e,

https://doi.org/10.1021/jacs.4c11866
J. Am. Chem. Soc. XXXX, XXX, XXX−XXX

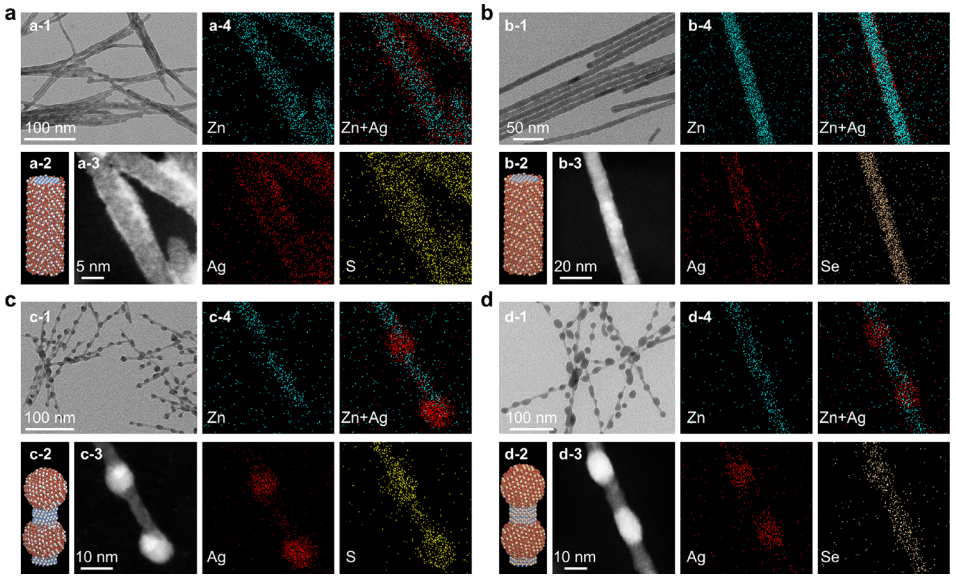

Figure 6. Generality of solid-state P-R instability in Ag-based chalcogenides Ag_2E (E = S, Se). (a–d) Characterization of ZnE@Ag_2E conformal core–shell heteronanowires (a, b) and –[ZnE@Ag_2E]-ZnE– periodically coaxial heteronanowires (c, d). (c-1, d-1) TEM image. (c-2, d-2) Schematic structure model. (c-3, d-3) HAADF-STEM image. (c-4, d-4) EDS elemental mapping images.

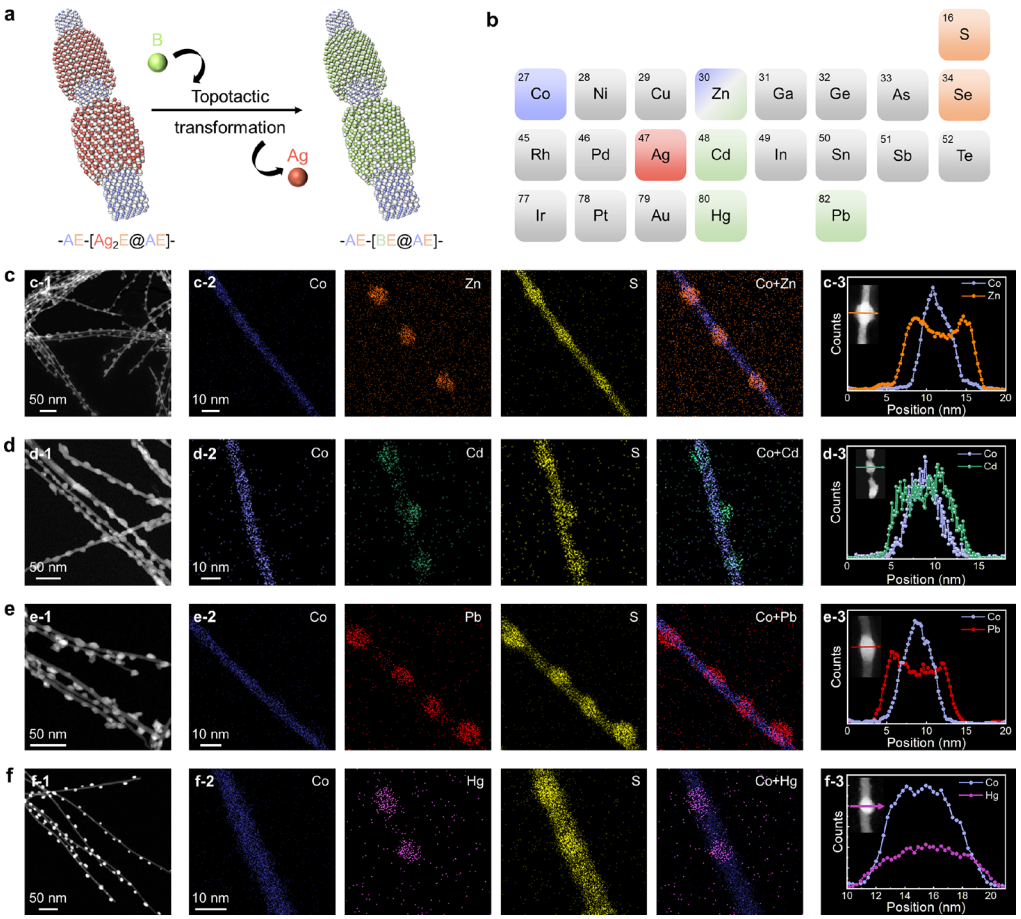

Figure 7. Topotactic transformations into a library of –[Co_9S_8@M_xS_y]-Co_9S_8– (M = Zn, Cd, Pb, Hg) periodically coaxial heteronanowires. (a) Schematic illustration of the topotactic transformation. (b) Library of chalcogenides involved in the transformations. (c–f) Characterization of a library of –[Co_9S_8@M_xS_y]-Co_9S_8– (M = Zn, Cd, Pb, Hg) periodically coaxial heteronnaowires. (c-1, d-1) HAADF-STEM image. (c-2, d-2) EDS elemental mapping images. (d-3, d-3) EDS line-scan profiles.

Figure S25, and Videos S4–S6). By contrast, for Ag_2S shells of subnanometer thicknesses, atoms in transition layers are frustrated and only suffer weak restraints from both the substrate and the bulk lattice, thus ensuring their high "fluidity".

https://doi.org/10.1021/jacs.4c11866
J. Am. Chem. Soc. XXXX, XXX, XXX–XXX

Nevertheless, the "fluidity" almost disappeared when converting the subnanometer Ag_2S shell into a rigid-lattice CdS shell with at least two-orders-of-magnitude smaller diffusion coefficients, as verified both experimentally (Figure S26a−c) and theoretically (Figure S26d−f and Video S7).

These results indicate that soft lattices and subnanometer thicknesses are two indispensable ingredients for the high "fluidity" of inorganic solids. Overall, we conclude that both thermodynamic and kinetic considerations are of equal importance for the observation of P-R instability in inorganic solids.

Synthetic Generality and Further Topotactic Transformation. Based on the above theoretical guidance, we then sought to examine the generality of such P-R instability in other cores of semiconductor nanowires and shells of silver-based chalcogenide ionic crystals. Given the large differences of cation radii and lattice parameters between Ag- and Zn-based chalcogenides, we took monodispersed ZnS nanowires as the 1D substrates (Figure S27a,b) and fabricated the ZnS@Ag_2S core−shell nanowires in a similar cation exchange approach, which feature the uniform Ag_2S shells with subnanometer thickness as well (Figure 6a and Figure S27c−f). We then postsynthetically transformed them into periodically coaxial −[ZnS@Ag_2S]-ZnS heteronanowires (Figure 6c and Figure S27g−m). In analogy, Ag_2Se shells of metastable ionic crystals can dewet from uniform ones into periodic ones on the 1D substrates of ZnSe nanowires (Figure 6b,d and Figure S28). HRTEM images (Figures S27i and S28h) and corresponding FFT images (Figures S27j and S28i) confirmed the epitaxial integration of cores and shells in those −[ZnE@Ag_2E]-ZnE− (E = S or Se) periodically coaxial heteronanowires, wherein the lattice-mismatch-induced interfacial strain energies drive such dewetting processes.

These results signify that the P-R instability may be a general, fundamental nature for soft inorganic solids and offers an exciting route toward high-order heterostructures that are inaccessible by conventional synthetic methodologies.

We highlight that these resulting high-order periodically coaxial heteronanowires can serve as key reaction intermediates for further topotactic transformations,[47−49] which enable integrating therein diverse functional subunits and thus create the periodically coaxial heteronanowire library.

As a proof of principle, we showcase the topotactic transformations on −[Co_9S_8@Ag_2S]-Co_9S_8− periodically coaxial heteronanowires via cation exchange reactions between the soft-acid Ag^+ and target hard-acid cations (Figure 7a). We therefore managed to integrate functional subunits with spectral absorption spanning from the UV, visible, and near-infrared regions to the mid-infrared region, yielding a library of −[Co_9S_8@M_xS_y]-Co_9S_8− (M = Zn, Cd, Pb, and Hg) periodically coaxial heteronanowires (Figure 7b−f and Figures S29 and S30). TEM images and HAADF images (Figure 7c−f and Figures S29a,c and S30a,b) show the uniform and well-conserved periodic morphology of all heteronanowires after the transformation.

XRD patterns (Figure S31), HRTEM images, and corresponding FFT images (Figures S29a−c and S30c,d) confirm the crystal structures of all M_xS_y semiconductor shells. Thanks to the topotactic transformation, the periodic shells present a well-defined epitaxial relationship between (111) planes of Co_9S_8 cores and (111) planes of the ZnS subunit (Figure S29a-2,a-3), (001) planes of the CdS subunit (Figure S30c,d), (222) of the PbS subunit (Figure S29b-2,b-3), and (222) planes of the HgS subunit (Figure S29c-2,c-3). We further confirmed the periodically coaxial structures by EDS elemental mapping images and EDS line-scan profiles (Figure 7c−f), implying that they were well-inherited from the −[Co_9S_8@Ag_2S]-Co_9S_8− periodically coaxial heteronanowires free from the lattice-matching rule.

Therefore, as compared to core−shell structures and single-component counterparts, this kind of periodic heterostructures are expected to exhibit unblocked optical absorption of solar irradiations by exposing both components, mitigated interfacial defects by reducing lattice distortions, engineerable band structures by vast material combinations, and steerable carrier transport by adjustable shell distances, thus holding exciting potentials for advanced applications in photoelectric and photochemical conversions.[29,30] To demonstrate the utility of these functional high-order heteronanowires, we further show, by taking −[Co_9S_8@CdS]-Co_9S_8− heteronanowires as an example due to their suitable band alignment, the potentials for solar-to-chemical conversions. We measured the optical band gap of plain Co_9S_8 nanowires to be ca. 2.25 eV according to the Tauc plot as transformed from the UV−vis diffuse reflectance spectrum (Figure S30g,h). Ultraviolet photoelectron spectroscopy (UPS) reveals that the valence band maximum of Co_9S_8 nanowires locates at 1.62 eV and the work function (Φ, the relative energy between the Fermi level and the vacuum level) is 4.49 eV (Figure S30i,j). Combining with the band energy structure of CdS,[50] we thus confirmed the type II energy band alignment between Co_9S_8 and CdS (Figure S30k), which would facilitate the charge separation at the heterointerface[51] and, therefore, improve the solar-to-fuel conversion efficiency. The Fermi level alignment was also confirmed by the increased binding energies of Co 2p core levels (Figure S30m−o). Thanks to the enhanced light-harvesting ability and superior charge-separation ability in such type II heterostructures, the −[Co_9S_8@CdS]-Co_9S_8− heteronanowires exhibited 40-fold and 6-fold higher photocurrent density during the photoelectrochemical hydrogen production reaction in alkaline electrolytes, respectively, as compared with plain Co_9S_8 nanowires and Co_9S_8@CdS conformal core−shell nanowires (Figure S30l).

The generality of P-R instability identified in silver chalcogenides together with the feasibility of further topotactic transformation translates to the access toward a broad range of functional periodic heteronanowires, which would hold great promise for applications in solar fuels, optoelectronics, and catalysis.

CONCLUSIONS

In conclusion, we report a general solid-state P-R instability of silver-based chalcogenide semiconductors (e.g., Ag_2S and Ag_2Se) of soft ionic solids, which enables the postsynthetic morphological transformations from conformal core−shell nanowires to periodically coaxial ones. Thermodynamically, the P-R instability occurs as a combinatorial result of surface and interface energy; kinetically, the high "fluidity" of solids for transformation is ensured by the subnanoscale soft-lattice ionic crystals. These findings enrich the concept of P-R instability in soft inorganic solids, which is expected to be general for other kinds of soft ionic crystals—for instance, perovskites[44]—and beyond.[45] It therefore offers a controllable approach for creating periodic nanostructures with improved or new functions, regulating the patterning at artificial all-inorganic solid−solid interfaces in devices, and fabricating flexible, deformable electronics.

https://doi.org/10.1021/jacs.4c11866
J. Am. Chem. Soc. XXXX, XXX, XXX−XXX

■ ASSOCIATED CONTENT

Supporting Information

The Supporting Information is available free of charge at https://pubs.acs.org/doi/10.1021/jacs.4c11866.

Calculation of strain energy and surface energy and molecular dynamics simulations (PDF)

Different heating times during the self-limited transformation process (MP4)

Ag_2S shells with different thicknesses (1.0, 2.0, and 10.0 nm) at different times (t = 0 and 10,000 ps) (MP4)

Ag_2S shells with different thicknesses (1.0, 2.0, and 10.0 nm) at different times (t = 0 and 10,000 ps) (MP4)

■ AUTHOR INFORMATION

Corresponding Authors

Huijun Jiang − *Key Laboratory of Precision and Intelligent Chemistry & Hefei National Research Center for Physical Sciences at the Microscale, University of Science and Technology of China, Hefei 230026, China;* orcid.org/0000-0001-7243-5431; Email: hjjiang3@ustc.edu.cn

Yi Li − *New Cornerstone Science Laboratory, Department of Chemistry, Institute of Biomimetic Materials and Chemistry, Anhui Engineering Laboratory of Biomimetic Materials, Division of Nanomaterials and Chemistry, Hefei National Research Center for Physical Sciences at the Microscale, University of Science and Technology of China, Hefei 230026, China; Anhui Province Engineering Research Center of Flexible and Intelligent Materials, School of Chemistry and Chemical Engineering, Hefei University of Technology, Hefei 230009, China*; Email: yili@hfut.edu.cn

Shu-Hong Yu − *New Cornerstone Science Laboratory, Department of Chemistry, Institute of Biomimetic Materials and Chemistry, Anhui Engineering Laboratory of Biomimetic Materials, Division of Nanomaterials and Chemistry, Hefei National Research Center for Physical Sciences at the Microscale, University of Science and Technology of China, Hefei 230026, China; Institute of Innovative Materials (I2M), Department of Chemistry, Department of Materials Science and Engineering, Southern University of Science and Technology, Shenzhen 518055, China;* orcid.org/0000-0003-3732-1011; Email: shyu@ustc.edu.cn

Authors

Zhen-Chao Shao − *New Cornerstone Science Laboratory, Department of Chemistry, Institute of Biomimetic Materials and Chemistry, Anhui Engineering Laboratory of Biomimetic Materials, Division of Nanomaterials and Chemistry, Hefei National Research Center for Physical Sciences at the Microscale, University of Science and Technology of China, Hefei 230026, China*

Xianyun Jiang − *Key Laboratory of Precision and Intelligent Chemistry & Hefei National Research Center for Physical Sciences at the Microscale, University of Science and Technology of China, Hefei 230026, China*

Chong Zhang − *New Cornerstone Science Laboratory, Department of Chemistry, Institute of Biomimetic Materials and Chemistry, Anhui Engineering Laboratory of Biomimetic Materials, Division of Nanomaterials and Chemistry, Hefei National Research Center for Physical Sciences at the Microscale, University of Science and Technology of China, Hefei 230026, China*

Tianhao Wang − *Key Laboratory of Precision and Intelligent Chemistry & Hefei National Research Center for Physical Sciences at the Microscale, University of Science and Technology of China, Hefei 230026, China*

Yan-Ru Wang − *The Instruments Center for Physical Science, University of Science and Technology of China, Hefei 230026, China*

Guo-Qiang Liu − *New Cornerstone Science Laboratory, Department of Chemistry, Institute of Biomimetic Materials and Chemistry, Anhui Engineering Laboratory of Biomimetic Materials, Division of Nanomaterials and Chemistry, Hefei National Research Center for Physical Sciences at the Microscale, University of Science and Technology of China, Hefei 230026, China*

Zong-Ying Huang − *Institute of Innovative Materials (I2M), Department of Chemistry, Department of Materials Science and Engineering, Southern University of Science and Technology, Shenzhen 518055, China*

Yu-Zhuo Zhang − *New Cornerstone Science Laboratory, Department of Chemistry, Institute of Biomimetic Materials and Chemistry, Anhui Engineering Laboratory of Biomimetic Materials, Division of Nanomaterials and Chemistry, Hefei National Research Center for Physical Sciences at the Microscale, University of Science and Technology of China, Hefei 230026, China*

Liang Wu − *New Cornerstone Science Laboratory, Department of Chemistry, Institute of Biomimetic Materials and Chemistry, Anhui Engineering Laboratory of Biomimetic Materials, Division of Nanomaterials and Chemistry, Hefei National Research Center for Physical Sciences at the Microscale, University of Science and Technology of China, Hefei 230026, China*

Zhong-Huai Hou − *Key Laboratory of Precision and Intelligent Chemistry & Hefei National Research Center for Physical Sciences at the Microscale, University of Science and Technology of China, Hefei 230026, China;* orcid.org/0000-0003-1241-7041

Complete contact information is available at: https://pubs.acs.org/10.1021/jacs.4c11866

Author Contributions

[§]Z.-C.S., X.J., and C.Z. contributed equally to this work.

Notes

The authors declare no competing financial interest.

■ ACKNOWLEDGMENTS

This work was supported by the National Natural Science Foundation of China (Grants 22293044, U1932213, 22271265, 22101270, 22405257, and 22373090), the National Key Research and Development Program of China (Grants 2021YFA0715700, 2018YFE0202201, and 2022YFA1303100), the Strategic Priority Research Program of the Chinese Academy of Sciences (Grants XDB0450402), the Natural Science Foundation Youth Project of Anhui Province (2108085QB74), USTC Research Funds of the Double First-Class Initiative (YD9990002013), the Major Basic Research Project of Anhui Province (2023z04020009), the Fundamental Research Funds for the Central Universities (WK2060000031, JZ2024HGPA0262), and the New Cornerstone Investigator Program. This work was partially carried out at the Instruments Center for Physical Science and the Center for Micro- and

Nanoscale Research and Fabrication, University of Science and Technology of China.

REFERENCES

(1) Parker, A. R.; Lawrence, C. R. Water capture by a desert beetle. *Nature* **2001**, *414*, 33−34.

(2) Zheng, Y.; Bai, H.; Huang, Z.; Tian, X.; Nie, F. Q.; Zhao, Y.; Zhai, J.; Jiang, L. Directional water collection on wetted spider silk. *Nature* **2010**, *463*, 640−643.

(3) Barthlott, W.; Neinhuis, C. Purity of the sacred lotus, or escape from contamination in biological surfaces. *Planta* **1997**, *202*, 1−8.

(4) Liu, M.; Wang, S.; Jiang, L. Nature-inspired superwettability systems. *Nat. Rev. Mater.* **2017**, *2*, 17036.

(5) Wang, S.; Liu, K.; Yao, X.; Jiang, L. Bioinspired Surfaces with Superwettability: New Insight on Theory, Design, and Applications. *Chem. Rev.* **2015**, *115*, 8230−8293.

(6) Plateau, J. A. F. Experimental and theoretical researches on the figures of equilibrium of a liquid mass withdrawn from the action of gravity.−Third series. *Annu. Rep. Smithson. Inst.* **1863**, 270−285.

(7) Rayleigh, L. On The Instability Of Jets. *Proc. London Math. Soc.* **1878**, *s1-10*, 4−13.

(8) Day, R. W.; Mankin, M. N.; Gao, R.; No, Y. S.; Kim, S. K.; Bell, D. C.; Park, H. G.; Lieber, C. M. Plateau-Rayleigh crystal growth of periodic shells on one-dimensional substrates. *Nat. Nanotechnol.* **2015**, *10*, 345−352.

(9) Day, R. W.; Mankin, M. N.; Lieber, C. M. Plateau-Rayleigh crystal growth of nanowire heterostructures: strain-modified surface chemistry and morphological control in one, two, and three dimensions. *Nano Lett.* **2016**, *16*, 2830−2836.

(10) Haefner, S.; Benzaquen, M.; Baumchen, O.; Salez, T.; Peters, R.; McGraw, J. D.; Jacobs, K.; Raphael, E.; Dalnoki-Veress, K. Influence of slip on the Plateau-Rayleigh instability on a fibre. *Nat. Commun.* **2015**, *6*, 7409.

(11) Wang, P.; Zhou, J.; Xu, B.; Lu, C.; Meng, Q.; Liu, H. Bioinspired Anti-Plateau-Rayleigh-Instability on Dual Parallel Fibers. *Adv. Mater.* **2020**, *32*, No. 2003453.

(12) Song, M.; Kartawira, K.; Hillaire, K. D.; Li, C.; Eaker, C. B.; Kiani, A.; Daniels, K. E.; Dickey, M. D. Overcoming Rayleigh-Plateau instabilities: Stabilizing and destabilizing liquid-metal streams via electrochemical oxidation. *Proc. Natl. Acad. Sci. U. S. A.* **2020**, *117*, 19026−19032.

(13) Wang, Z.; He, B.; Xu, G.; Wang, G.; Wang, J.; Feng, Y.; Su, D.; Chen, B.; Li, H.; Wu, Z.; et al. Transformable masks for colloidal nanosynthesis. *Nat. Commun.* **2018**, *9*, 563.

(14) Zhan, Y.-J.; Yu, S.-H. Necklace-Like Cu@Cross-Linked Poly (vinyl alcohol) Core−Shell Microcables by Hydrothermal Process. *J. Am. Chem. Soc.* **2008**, *130*, 5650−5651.

(15) Wang, X.; Zhang, M.-Q.; Kou, R.; Lu, L.-L.; Zhao, Y.; Xu, X.-W.; Liu, G.-M.; Zheng, Y.-M.; Yu, S.-H. Unique Necklace-Like Phenol Formaldehyde Resin Nanofibers: Scalable Templating Synthesis, Casting Films, and Their Superhydrophobic Property. *Adv. Funct. Mater.* **2016**, *26*, 5086−5092.

(16) Xue, Z.; Xu, M.; Zhao, Y.; Wang, J.; Jiang, X.; Yu, L.; Wang, J.; Xu, J.; Shi, Y.; Chen, K.; et al. Engineering island-chain silicon nanowires via a droplet mediated Plateau-Rayleigh transformation. *Nat. Commun.* **2016**, *7*, 12836.

(17) Li, P.; Han, Y.; Zhou, X.; Fan, Z.; Xu, S.; Cao, K.; Meng, F.; Gao, L.; Song, J.; Zhang, H.; et al. Thermal Effect and Rayleigh Instability of Ultrathin 4H Hexagonal Gold Nanoribbons. *Matter* **2020**, *2*, 658−665.

(18) Karim, S.; Toimil-Molares, M. E.; Balogh, A. G.; Ensinger, W.; Cornelius, T. W.; Khan, E. U.; Neumann, R. Morphological evolution of Au nanowires controlled by Rayleigh instability. *Nanotechnology* **2006**, *17*, 5954−5959.

(19) Ferraro, P.; Coppola, S.; Grilli, S.; Paturzo, M.; Vespini, V. Dispensing nano-pico droplets and liquid patterning by pyroelectrodynamic shooting. *Nat. Nanotechnol.* **2010**, *5*, 429−435.

(20) Kaufman, J. J.; Tao, G.; Shabahang, S.; Banaei, E. H.; Deng, D. S.; Liang, X.; Johnson, S. G.; Fink, Y.; Abouraddy, A. F. Structured spheres generated by an in-fibre fluid instability. *Nature* **2012**, *487*, 463−467.

(21) Gumennik, A.; Wei, L.; Lestoquoy, G.; Stolyarov, A. M.; Jia, X.; Rekemeyer, P. H.; Smith, M. J.; Liang, X.; Grena, B. J.; Johnson, S. G.; et al. Silicon-in-silica spheres via axial thermal gradient in-fibre capillary instabilities. *Nat. Commun.* **2013**, *4*, 2216.

(22) Song, H.; Ismagilov, R. F. Millisecond Kinetics on a Microfluidic Chip Using Nanoliters of Reagents. *J. Am. Chem. Soc.* **2003**, *125*, 14613−14619.

(23) Tian, X.; Chen, Y.; Zheng, Y.; Bai, H.; Jiang, L. Controlling water capture of bioinspired fibers with hump structures. *Adv. Mater.* **2011**, *23*, 5486−5491.

(24) Bai, H.; Ju, J.; Zheng, Y.; Jiang, L. Functional fibers with unique wettability inspired by spider silks. *Adv. Mater.* **2012**, *24*, 2786−2791.

(25) Liu, Z.; Qi, D.; Hu, G.; Wang, H.; Jiang, Y.; Chen, G.; Luo, Y.; Loh, X. J.; Liedberg, B.; Chen, X. Surface Strain Redistribution on Structured Microfibers to Enhance Sensitivity of Fiber-Shaped Stretchable Strain Sensors. *Adv. Mater.* **2018**, *30*, No. 1704229.

(26) Song, J.; Zhang, W.; Wang, D.; Fan, Y.; Zhang, C.; Wang, D.; Chen, L.; Miao, B.; Cui, J.; Deng, X. Polymeric Microparticles Generated via Confinement-Free Fluid Instability. *Adv. Mater.* **2021**, *33*, No. 2007154.

(27) Lin, Q. Y.; Mason, J. A.; Li, Z.; Zhou, W.; O'Brien, M. N.; Brown, K. A.; Jones, M. R.; Butun, S.; Lee, B.; Dravid, V. P.; Aydin, K.; Mirkin, C. A. Building superlattices from individual nanoparticles via template-confined DNA-mediated assembly. *Science* **2018**, *359*, 669−672.

(28) Zhang, Z.; Huang, Z.; Li, J.; Wang, D.; Lin, Y.; Yang, X.; Liu, H.; Liu, S.; Wang, Y.; Li, B.; et al. Endoepitaxial growth of monolayer mosaic heterostructures. *Nat. Nanotechnol.* **2022**, *17*, 493−499.

(29) Li, Y.; Zhang, C.; Zhuang, T.-T.; Lin, Y.; Tian, J.; Qi, X.-Y.; Li, X.; Wang, R.; Wu, L.; Liu, G.-Q.; et al. One-Dimensional Superlattice Heterostructure Library. *J. Am. Chem. Soc.* **2021**, *143*, 7013−7020.

(30) Li, Y.; Zhuang, T.-T.; Zhang, C.; Wu, L.; Han, S.-K.; Yu, S.-H. Axially Segmented Semiconductor Heteronanowires. *Acc. Mater. Res.* **2020**, *1*, 126−136.

(31) Lu, Q.; Wang, A. L.; Gong, Y.; Hao, W.; Cheng, H.; Chen, J.; Li, B.; Yang, N.; Niu, W.; Wang, J.; et al. Crystal phase-based epitaxial growth of hybrid noble metal nanostructures on 4H/fcc Au nanowires. *Nat. Chem.* **2018**, *10*, 456−461.

(32) Zhao, B.; Wan, Z.; Liu, Y.; Xu, J.; Yang, X.; Shen, D.; Zhang, Z.; Guo, C.; Qian, Q.; Li, J.; et al. High-order superlattices by rolling up van der Waals heterostructures. *Nature* **2021**, *591*, 385−390.

(33) Teitsworth, T. S.; Hill, D. J.; Litvin, S. R.; Ritchie, E. T.; Park, J.-S.; Custer, J. P.; Taggart, A. D.; Bottum, S. R.; Morley, S. E.; Kim, S.; et al. Water splitting with silicon p-i-n superlattices suspended in solution. *Nature* **2023**, *614*, 270−274.

(34) Wang, C.; He, Q.; Halim, U.; Liu, Y.; Zhu, E.; Lin, Z.; Xiao, H.; Duan, X.; Feng, Z.; Cheng, R.; et al. Monolayer atomic crystal molecular superlattices. *Nature* **2018**, *555*, 231−236.

(35) De Trizio, L.; Manna, L. Forging Colloidal Nanostructures via Cation Exchange Reactions. *Chem. Rev.* **2016**, *116*, 10852−10887.

(36) Sun, Y.; Wang, Y.; Chen, J. Y. C.; Fujisawa, K.; Holder, C. F.; Miller, J. T.; Crespi, V. H.; Terrones, M.; Schaak, R. E. Interface-mediated noble metal deposition on transition metal dichalcogenide nanostructures. *Nat. Chem.* **2020**, *12*, 284−293.

(37) Shi, X.; Chen, H.; Hao, F.; Liu, R.; Wang, T.; Qiu, P.; Burkhardt, U.; Grin, Y.; Chen, L. Room-temperature ductile inorganic semiconductor. *Nat. Mater.* **2018**, *17*, 421−426.

(38) Ren, Q.; Gupta, M. K.; Jin, M.; Ding, J.; Wu, J.; Chen, Z.; Lin, S.; Fabelo, O.; Rodriguez-Velamazan, J. A.; Kofu, M.; et al. Extreme phonon anharmonicity underpins superionic diffusion and ultralow thermal conductivity in argyrodite Ag_8SnSe_6. *Nat. Mater.* **2023**, *22*, 999−1006.

(39) Haynes, W. M.; Lide, D. R.; Bruno, T. J. *Handbook of Chemistry and Physics*, 97th ed.; CRC Press: Boca Raton, 2016.

(40) Li, Y.; Shao, Z. C.; Zhang, C.; Yu, S. H. Catalyzed Growth for Atomic-Precision Colloidal Chalcogenide Nanowires and Heterostructures: Progress and Perspective. *J. Phys. Chem. Lett.* **2021**, *12*, 10695−10705.

https://doi.org/10.1021/jacs.4c11866
J. Am. Chem. Soc. XXXX, XXX, XXX−XXX

(41) Li, G.; An, Q.; Morozov, S. I.; Duan, B.; Goddard, W. A.; Zhang, Q.; Zhai, P.; Snyder, G. J. Ductile deformation mechanism in semiconductor α-Ag_2S. *npj Comput. Mater.* **2018**, *4*, 44.
(42) Carbone, L.; Cozzoli, P. D. Colloidal heterostructured nanocrystals: Synthesis and growth mechanisms. *Nano Today* **2010**, *5*, 449−493.
(43) Ji, B.; Panfil, Y. E.; Waiskopf, N.; Remennik, S.; Popov, I.; Banin, U. Strain-controlled shell morphology on quantum rods. *Nat. Commun.* **2019**, *10*, 2.
(44) Li, X.; Meng, Y.; Li, W.; Zhang, J.; Dang, C.; Wang, H.; Hung, S.-W.; Fan, R.; Chen, F.-R.; Zhao, S.; et al. Multislip-enabled morphing of all-inorganic perovskites. *Nat. Mater.* **2023**, *22*, 1175−1181.
(45) Wei, T. R.; Jin, M.; Wang, Y.; Chen, H.; Gao, Z.; Zhao, K.; Qiu, P.; Shan, Z.; Jiang, J.; Li, R.; Chen, L.; He, J.; Shi, X. Exceptional plasticity in the bulk single-crystalline van der Waals semiconductor InSe. *Science* **2020**, *369*, 542−545.
(46) Chen, H.; Wei, T. R.; Zhao, K.; Qiu, P.; Chen, L.; He, J.; Shi, X. Room-temperature plastic inorganic semiconductors for flexible and deformable electronics. *InfoMater.* **2021**, *3*, 22−35.
(47) Feng, Y.; Ji, Y.; Zhang, Y.; Shao, Q.; Xu, Y.; Li, Y.; Huang, X. Synthesis of noble metal chalcogenides via cation exchange reactions. *Nat. Synth.* **2022**, *1*, 626−634.
(48) Loiudice, A.; Buonsanti, R. Reaction intermediates in the synthesis of colloidal nanocrystals. *Nat. Synth.* **2022**, *1*, 344−351.
(49) Fenton, J. L.; Steimle, B. C.; Schaak, R. E. Tunable intraparticle frameworks for creating complex heterostructured nanoparticle libraries. *Science* **2018**, *360*, 513−517.
(50) Lian, Z.; Kobayashi, Y.; Vequizo, J. J. M.; Ranasinghe, C. S. K.; Yamakata, A.; Nagai, T.; Kimoto, K.; Kobayashi, K.; Tanaka, K.; Teranishi, T.; et al. Harnessing infrared solar energy with plasmonic energy upconversion. *Nat. Sustain.* **2022**, *5*, 1092−1099.
(51) Sitt, A.; Hadar, I.; Banin, U. Band-gap engineering, optoelectronic properties and applications of colloidal heterostructured semiconductor nanorods. *Nano Today* **2013**, *8*, 494−513.

https://doi.org/10.1021/jacs.4c11866
J. Am. Chem. Soc. XXXX, XXX, XXX−XXX